PROFILING DESIGN AND OPTIMIZATION OF END-EFFECTOR FOR PINEAPPLE EYE REMOVAL
/
菠萝去眼末端执行机构仿形设计与优化

Xingzao MA, Manfeng GONG*), Hua LI, Shuai WANG
School of Mechanical and Electrical, Lingnan Normal University, Zhanjiang 524048, China
Tel: 13414898351; E-mail: gongmanfeng@163.com
DOI: https://doi.org/10.35633/inmateh-76-76

Keywords: *pineapple, end-effector, profiling design, structural optimization design, finite element analysis, pineapple eye removal device*

ABSTRACT
To address the issues of high labor intensity, low efficiency, and excessive flesh loss in pineapple eye removal, a design scheme of pineapple eye removal end-effector based on mechanical arm was proposed according to the analysis results of pineapple eye morphological characteristics. Based on the experimental determination of the elastic modulus of the pineapple fruit eye area, the design of the end-effector mechanism for pineapple eye removal, kinematic and dynamic simulation analysis, and finite element optimization design of the eye removal gripper were carried out. Finally, a pineapple eye removal device was built for experimental verification. The simulation results indicated that the optimal length of the driving link of the pineapple eye removal end-effector mechanism was 23 mm. The eye removal trajectory of the gripper tip was highly consistent with the morphological contours of pineapple eyes. The maximum contact forces between gears and at the gripper-pineapple interface reached 33.13 N and 78.64 N, respectively. Under this condition, the maximum stress and maximum deformation of the gripper tip were 532.15 MPa and 0.17 mm, respectively, and there was a significant stress concentration phenomenon. After structural optimization, the maximum stress and deformation were reduced to 133.13 MPa and 0.12 mm, with reduction rates of approximately 75% and 29.4%, respectively. These improvements effectively enhanced the structural stress distribution and deformation behavior, meeting the material strength requirements. The experimental results showed that pineapple eye removal operations were efficiently completed by the end-effector mechanism, with an eye removal success rate of 98%. The research results provide theoretical and technical reference for the development of pineapple automatic processing equipment.

摘要
针对菠萝去眼劳动强度大、效率低、果肉损耗率偏高等问题，依据菠萝果眼形态特征分析结果，提出了一种基于机械臂的菠萝去眼末端执行机构设计方案。在试验测定菠萝果眼区域的弹性模量的基础上，开展菠萝去眼末端执行机构设计、运动学与动力学仿真分析及去眼手爪有限元优化设计，最后搭建菠萝去眼装置进行试验验证。仿真结果表明，菠萝去眼末端执行机构的原动件杆最优杆长为 23 mm，手爪尖点的去眼轨迹与菠萝果眼形态高度吻合，齿轮间最大接触力达 33.13 N，手爪与菠萝最大接触力为78.64 N，在此工况下，手爪尖点的最大应力与最大变形量分别为532.15 MPa 和0.17 mm，存在显著的应力集中现象。经结构优化后，最大应力和最大变形分别为 133.13 MPa 和 0.12 mm，降幅分别约为 75%和 29.4%，有效改善了结构应力分布与变形情况，满足材料强度要求。试验结果显示，该末端执行机构可高效完成菠萝去眼作业，去眼成功率达 98%。研究成果可为菠萝自动化加工装备研发提供理论支撑与技术参考。

INTRODUCTION
Pineapples are rich in nutrients, including fructose and vitamins, and have a unique flavor that is widely appreciated (*Deng et al., 2018*). However, fresh pineapples have a short shelf life, and their market prices vary significantly. To provide growers with stable income, most harvested pineapples were processed (*Fang, 2023; Gong, 2020*), with eye removal being the most time-consuming and labor-intensive aspect of post-harvest handling (*Liu et al., 2022*).

To date, numerous researchers have reported advancements in machinery for pineapple eye removal. *Kumar P. (2021)* developed a new device for easing the process specifically for removing eyes and evaluated the device by compared with the present tool. *Liu (*2020*) designed* a novel pineapple eye removal device based on a V-shaped blade, which performs eye removal by pulling the handle to enhance operational smoothness. *Zhang et al (2018)* from Dezhou University developed a "Detachable Pineapple Peeling and Eye Removal Machine" and *Wen et al (2021)* from Tianjin University of Technology designed a "Pineapple Peeling

and Eye Removal Machine". Both schemes achieved semi-mechanized peeling and eye removal through innovative structural designs. Such devices have a simple structure, low working efficiency, and high labor intensity, making them unsuitable for widespread adoption.

With the development and maturation of computer image processing, artificial intelligence, and electronic technology, some researchers have integrated computer vision technology with the requirements of pineapple eye removal. *Trieu N. M. et al (2022)* designed an automatic pineapple eye removal machine that fixed the pineapple in place, used a camera to identify the eye positions, and removed them with a rotating cutter. Additionally, *Zhang et al (2021)* from the Institute of Automation, Chinese Academy of Sciences, invented the "Automatic Pineapple Eye Removal Device," which automates mechanical peeling and eye removal. This device employed a camera to recognize the spiral trajectory of the pineapple eyes, generating control instructions to guide the pineapple knife along the spiral path to remove the eyes. *Liu et al (2024)* designed a machine for automatic pineapple eye removal based on machine vision, which used an industrial camera to identify pineapple eyes. The modified eye removal forceps were mounted on a tool-closing cylinder, and the eye removal function was realized through the operation of the closing cylinder. *Gong et al. (2025)* used a depth camera to locate the pineapple eyes and installed the eye-removal gripper on the XZ-axis sliding platform to realize the pineapple eye removal operation. *Qian et al (2024)* used 3D reconstruction technology to acquire surface data of the pineapple and applied a trajectory-searching algorithm to obtain the trajectory path. The tool was then guided along the planned trajectory to perform spiral eye removal on the pineapple. However, existing research on pineapple eye removal predominantly concentrates on operational implementation and process control, whereas systematic studies focusing on the optimization design of the end-effector mechanism itself are rarely addressed.

With the excellent flexibility, environmental adaptability and high-precision operation characteristics，the mechanical arm demonstrates significant advantages in reducing labor costs and enhancing production efficiency, while exhibiting application potential for multi-machine collaborative operation *(Wu et al., 2024; Li et al., 2024; Duan et al., 2021; Zhang et al., 2024)*. However, the research on the application of pineapple eye removal is still blank. Therefore, a mechanical-arm-based end-effector mechanism design for pineapple eye removal was proposed in this study. Specifically, 3D modeling was accomplished using SolidWorks; kinematic and dynamic simulation analyses were conducted via ADAMS software; structural optimization of the removal gripper was implemented through ANSYS finite element analysis; and a pineapple eye removal test device was ultimately constructed for experimental validation. The research results can provide theoretical support and technical guidance for the design and manufacture of pineapple eye removal equipment and addressing key technical challenges in this field.

MATERIALS AND METHODS

Physical properties of pineapple

China has a diverse range of pineapple varieties, with the Bali variety occupying the largest planting area, accounting for approximately 76% of total pineapple cultivation. This variety currently serves as the primary source for pineapple processing (*Jin, 2021*). The pineapples used in this experiment were purchased from farmers near Zhanjiang City, Guangdong Province, in early January. Forty pineapples with varying degrees of maturity and sizes were selected for morphological measurements, as detailed in Table 1. To ensure the eye-removal gripper conformed to the shape of the pineapple eyes and achieved optimal removal efficiency, measurements were taken of the physical characteristics of the pineapple eye area, including cross-sectional shape, depth range, angle range, and elastic modulus.

Table 1

Statistical table of characteristic parameters of pineapple (Bali)

Unpeeled mass [g]	Peeled mass [g]	Fruit longitudinal diameter [mm]	Fruit equatorial diameter [mm]	Number of fruit eyes
1252.5±187	897.5±162	124.7±12.7	105.94±5.5	97±7

Shape characteristics of pineapple eye

The structure of the pineapple fruit, as shown in Figure 1, was radially divided into three concentric layers from the interior to the exterior: the core, pulp, and eye. The core had a compact structure, while the pulp layer was relatively loose. The eye layer formed the outermost surface of the pulp, encompassing the entire fruit.

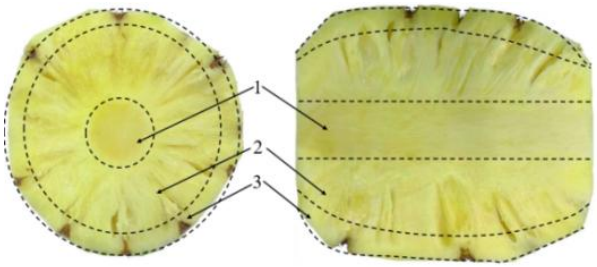

a. Radial cross-section **b. Axial cross-section**

Fig. 1 - Pineapple fruit structure

1-core area; 2-pulp area; 3-eye area.

Pineapples were classified into three ripeness stages: early ripening stage, mid ripening stage, and late ripening stage. Cross-sectional images of pineapple eyes at each maturity stage were presented in Figure 2. The shape of pineapple eyes remained generally consistent across different ripeness stages. Examination of individual pineapple eye profiles revealed a structure characterized by a frustum shape at the top and a cone-shaped pit at the base, with a distinct dark brown color. A total of 300 pineapple eyes representing the different ripeness stages were selected, and their depth and cone angles were measured. The depth and cone angle ranges of the pineapple eyes were shown in Figures 3 and 4, respectively.

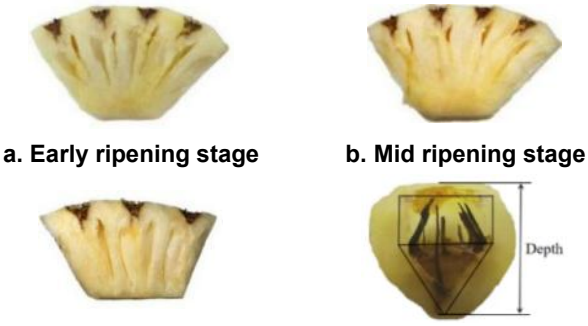

a. Early ripening stage **b. Mid ripening stage**

c. Late ripening stage **d. Single fruit eye**

Fig. 2 -Cross-section of a pineapple eye

As shown in Figures 3 and 4, the depth of the pineapple eyes was primarily distributed between 9~10 mm, with a maximum depth of 13 mm. The angle distribution mainly fell between 28°~32°, reaching a maximum angle of 40°. In the structural design, to meet the design requirements and ensure the complete removal of all pineapple eyes, the depth of the eye-removal gripper on the end-effector had to be at least 13 mm, with an angle of no less than 40°.

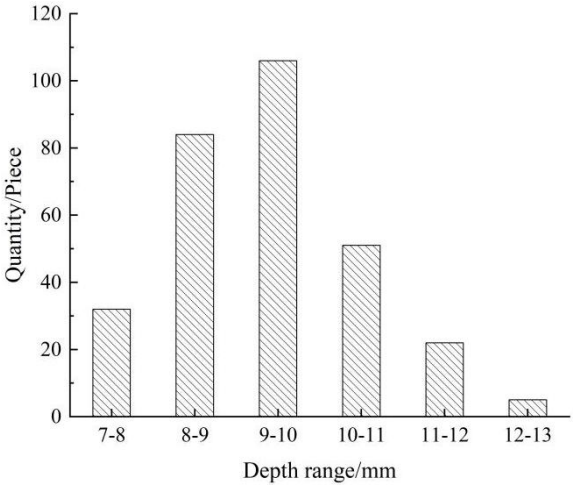

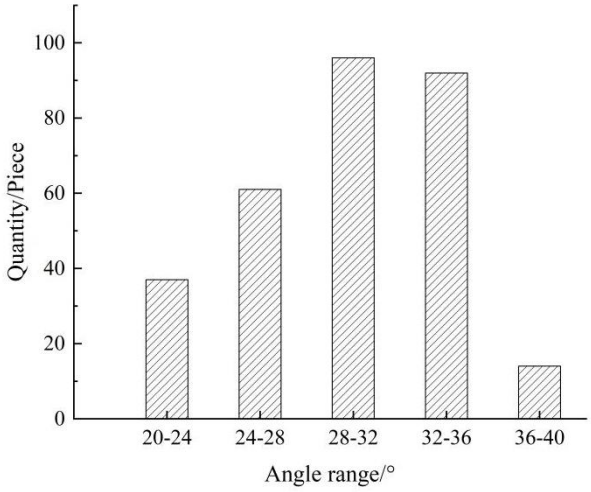

Fig. 3 -Depth distribution diagram of pineapple eyes **4 -Angle distribution diagram of pineapple eyes**

Compression test

The compression test was conducted using an electronic universal testing machine (MTS Exceed E43) with a maximum load capacity of 10 kN and an effective compression space of 1000 mm. A rigid plate indenter was employed, and the loading rate was maintained at 1 mm/min. Compression tests were performed on samples taken from the eye area, pulp area, and core area of each pineapple, as shown in Figure 5. Collected data were analyzed to calculate the elastic modulus for different regions of the pineapple at each maturity stage. The test results were presented in Figure 6.

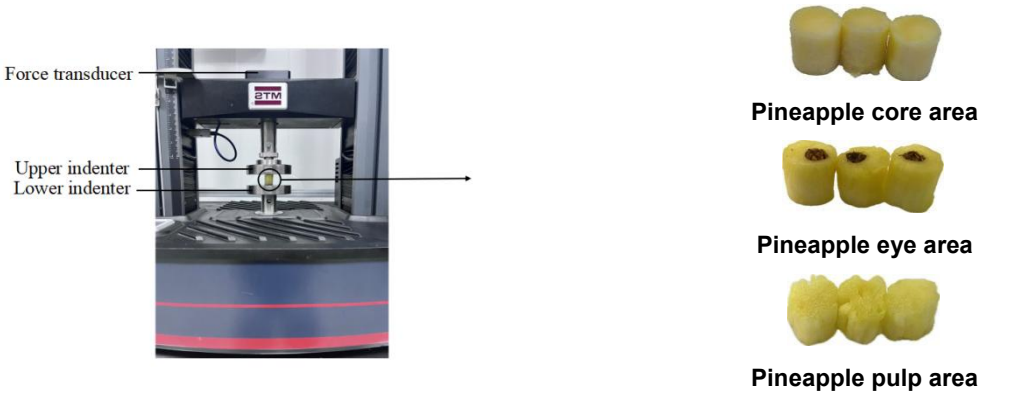

a. Compression test apparatus **b. Compression test sample**

Fig. 5 - Compression test

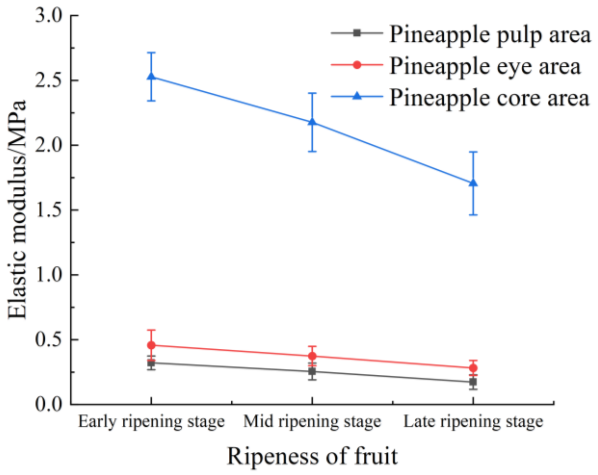

Fig. 6 -Elastic modulus of different regions of pineapple

Figure 6 showed that under identical ripeness conditions, the elastic modulus of the core region was significantly higher than that of the other two regions, while the eye and flesh regions exhibited little difference in elastic modulus. Elastic modulus across regions differed substantially among pineapples of varying ripeness. Early ripening pineapples demonstrated higher elastic modulus in all regions compared to other ripeness levels, with the highest value of 2.53 MPa observed in the early ripening core region. Conversely, the lowest modulus of 0.17 MPa occurred in the flesh of late ripening pineapples. These experimental results aligned with conclusions from compression tests on pineapples reported by *Xue Zhong et al. (2024)* from the Chinese Academy of Tropical Agricultural Sciences. Since mid-ripening pineapples dominated industrial processing, this study adopted the elastic modulus of the eye region (0.37 MPa) in mid ripening pineapples as the ADAMS simulation parameter.

The overall structure scheme

Based on the morphological characteristics of the pineapple eye, which featured a frustum-shaped top and a conical depression at the base, with a maximum depth of 13 mm and a base cone angle of 40°, the eye-removal gripper of the end-effector was designed with a profiling approach to match this shape and enhance

removal efficiency. Drawing inspiration from the pineapple eye's geometry, a pyramidal configuration was adopted, resulting in a semi-conical shape for the gripper. The dimensions were adjusted to fit the pineapple eye, with a depth of 15 mm and an angle of 21° to meet the design specifications. The opening and closing motion of the gripper was regulated by a gear mechanism, to which it was attached via a revolute joint. To ensure consistent motion, a limiting component was incorporated between the gripper and the gear mechanism to restrict its movement trajectory. The end-effector is shown in Figure 7.

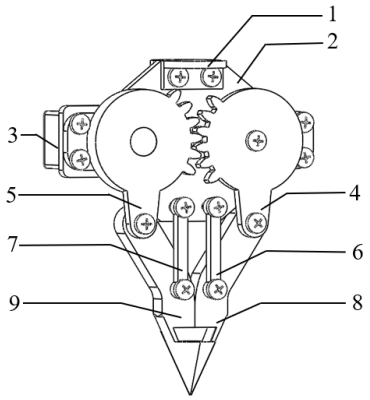

Fig. 7 - Schematic diagram of the end-effector

1- Clasp; 2-Bottom board; 3-Camel; 4-First gear mechanism; 5-Second gear mechanism; 6-First limit switch; 7-Second limit switch; 8-First eye removal gripper; 9-Second eye removal gripper

Structural parameter design

Since the designed end-effector was symmetrical about the central plane, the structure on one side of the centerline was selected for analysis (*Ye et al., 2011*). The structural diagram of the mechanism was shown in Figure 8, based on the configuration depicted in Figure 7.

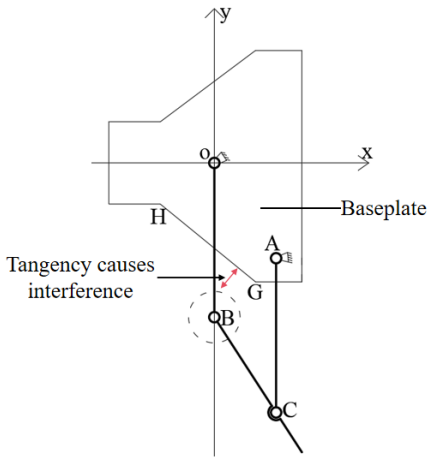

Fig. 8 - Structural diagram of the eye removal end-effector

Points O and A were fixed joints, consisting of the gear mechanism, limit element, and base plate, respectively. Points B and C were rotating joints, comprising the gear mechanism, limit element, and eye-removal gripper. HG represented the lower bevel of the base plate. As illustrated in Figure 9, when the length of the OB rod decreased below a certain value, interference occurred between the BC rod and the lower bevel HG of the base plate, thus requiring a minimum length for the BC rod. The rod width was modeled as a circle centered at point B with a radius of 5 mm. When this circle was tangent to the bevel HG, the BC rod was at its minimum achievable length. A rectangular coordinate system was established with point O as the origin. Given the coordinates of point H as (x_1,y_1) and point G as (x_2,y_2), the slope k of line l_{GH} was determined by:

$$k = \frac{y_2 - y_1}{x_2 - x_1} \tag{1}$$

Considering that the linear equation of l_{GH} was:

$$y - y_1 = k(x - x_1) \tag{2}$$

Point B was located on the y-axis, with coordinates $(0,y)$. According to the formula for the distance from a point to a line

$$d = \frac{|Ax_0 + By_0 + C|}{\sqrt{A^2 + B^2}} \quad (3)$$

Substituting the coordinates of point H (-10.5, 8.0) and point G (8.0, -22.5) yielded

$$y \approx -22.58 \text{ mm} \quad (4)$$

Therefore, the length of the OB rod was required to be at least 22.58 mm. It was rounded, and 23 mm was selected as its rod length.

The movement of the pineapple eye-removal gripper was controlled by a gear mechanism, where the rotation angle of the gear influenced the opening and closing distance of the gripper. Consequently, the relationship between the rotation angle of the gear and the opening and closing distance of the gripper was analyzed. The motion diagram for this mechanism was shown in Figure 9.

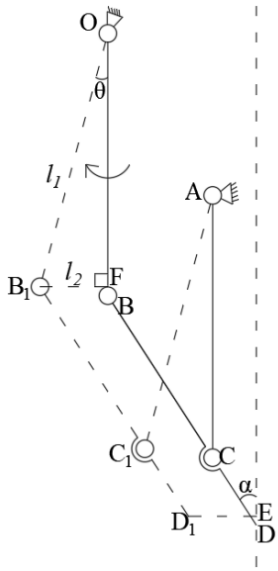

Fig. 9 - Motion diagram of the eye removal end-effector

In the figure, point D represented the initial position of the eye-removal gripper. Points B_1, C_1, and D_1 denoted the positions of points B, C, and D, respectively, after the OB rod had rotated by an θ angle. Point F was the perpendicular projection of B_1 onto the OB rod, while point E was the perpendicular projection of D_1 onto the central axis. The length of the OB rod was denoted as l_1, and the length of B_1F was denoted as l_2. Establishing the relationship between the rotation angle and the opening-closing distance was equivalent to identifying the relationship between the length D_1E and the parameter θ. The OB rod was parallel and equal in length to the AC rod. When the OB rod rotated by an angle θ, the AC rod rotated by the same angle θ under the motion of the OB rod, which results in the following relationship:

$$l_{D_1E} = l_{B_1F} = l_2 \quad (5)$$

In the right triangle OB_1F:

$$l_2 = l_1 \times \sin\theta \quad (6)$$

Thus, it was calculated:

$$\theta = arc\,sin\frac{l_2}{l_1} \quad (7)$$

Simulation optimization of rod length

Since the pineapple eye removal end-effector mechanism could not operate independently and required integration with a mechanical arm, a simplified test device was constructed. Based on the motion requirements and parameter settings of each structure, 3D modeling was completed in SolidWorks. After simplification, the model was imported into ADAMS (*Xia et al., 2021*).

Within ADAMS, material properties, constraints, external forces, and other factors were applied to various model components, and dynamic parameters were defined. The main body of the prototype model utilized aluminum alloy material. Physical property parameters for the pineapple were based on data obtained from compression tests, with material parameters listed in Table 2. The virtual prototype was shown in Figure 10. To optimize the OB link length, a series of simulations were performed in ADAMS software according to actual pineapple eye removal paths. By controlling two variables—eye removal time and rotational angular velocity—simulations for different link lengths were conducted to analyze the influence of driving link length on contact forces during eye removal and gear torque. This methodology determined the optimal OB link length. As previously analyzed, the minimum achievable OB link length was 22.58 mm. Considering practical constraints, this value was rounded to 23 mm. Starting from this minimum length as the initial value, the link length was incremented by 5 mm in successive simulations until reaching 43 mm. Simulation results for different link lengths were presented in Figure 11.

Table 2

Material property parameters

Parameter type	Aluminum alloy	Pineapple fruit eye
Material density [kg·m^{-3}]	7.85×10^{3}	1.09×10^{3}
Elastic modulus [MPa]	$2.\times10^{5}$	0.37
Poisson ratio	0.3	0.46

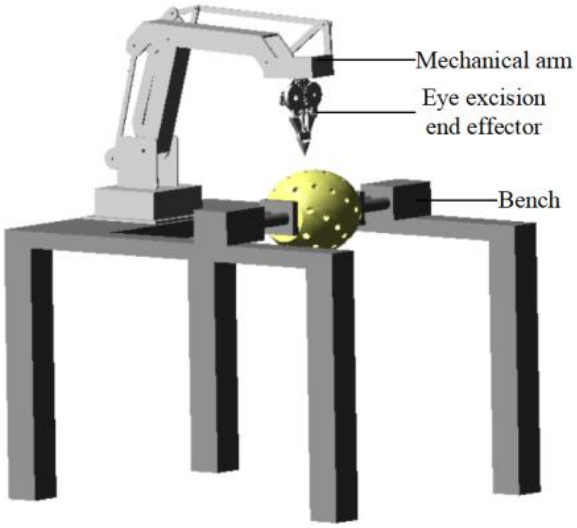

Fig. 10 - Virtual prototype built based on ADAMS

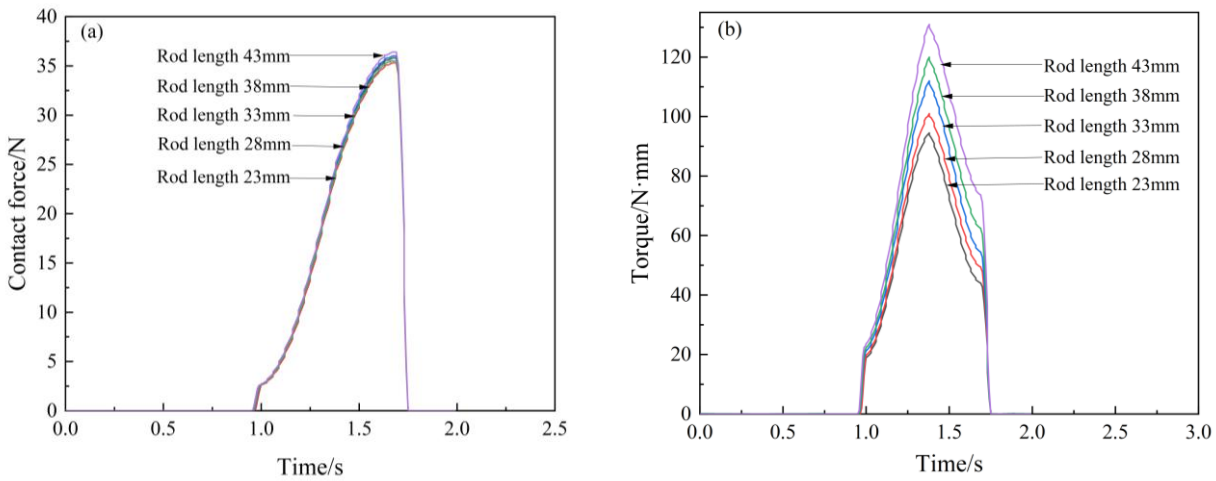

a. Eye removal time was the same

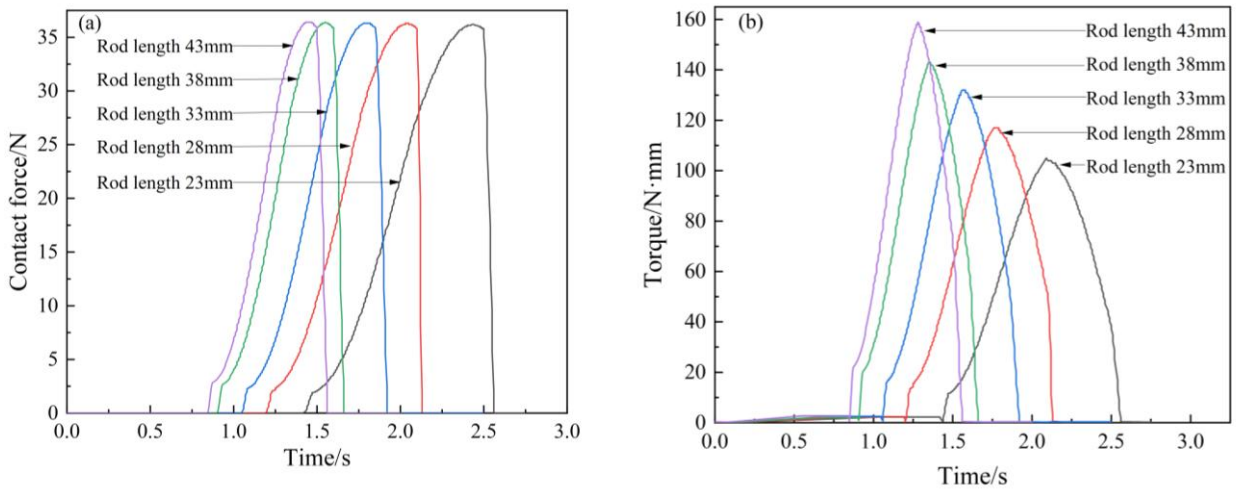

b. Rotational angular velocity was the same

Fig. 11 - Simulation results of different rod lengths

Figure 11 showed that when eye removal time or rotational angular velocity remained constant, contact forces were insensitive to changes in link length, while torque increased with longer link lengths. Simulation results revealed that shorter link lengths required lower torque, indicating that the minimum achievable OB link length constituted the optimal design length.

Kinematic and Dynamic Simulation Analysis

Within the ADAMS Simulation module, appropriate driving functions were applied to the prototype. The simulation time was set to 7 seconds with 2000 steps, modeling eye removal operations at three different locations. During the eye removal process, the gripper opened to a suitable angle via gear mechanism rotation. Driven by the mechanical arm, it positioned itself within the eye region. Upon reaching the top of the conical eye pit, the gripper closed to separate the pineapple eye. Following gripper closure, the mechanical arm rapidly ascended to complete the operation. The eye removal trajectory was shown in Figure 12.

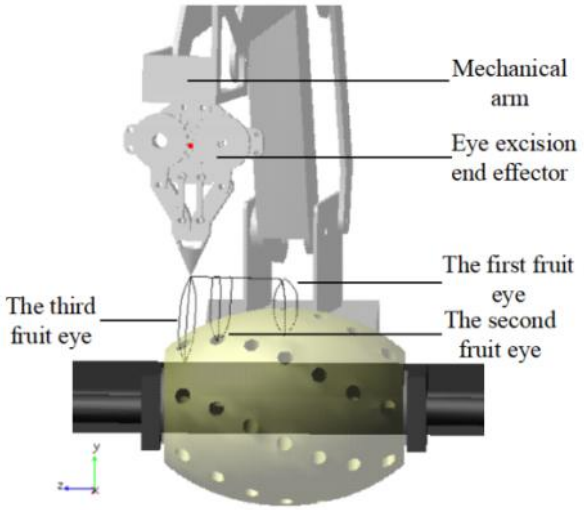

Fig. 12 - Eye removal trajectory

Figure 12 showed that the eye removal trajectory of the gripper tip highly aligned with the morphological profile of the pineapple eye, demonstrating the rationality of the designed end-effector solution.

To obtain mechanical parameters at critical positions during pineapple eye removal, the kinematics and dynamics simulation analysis of the contact force between the gears and the contact force between the eye removal gripper and the pineapple were carried out. The simulation results were shown in Figures 13 and 14.

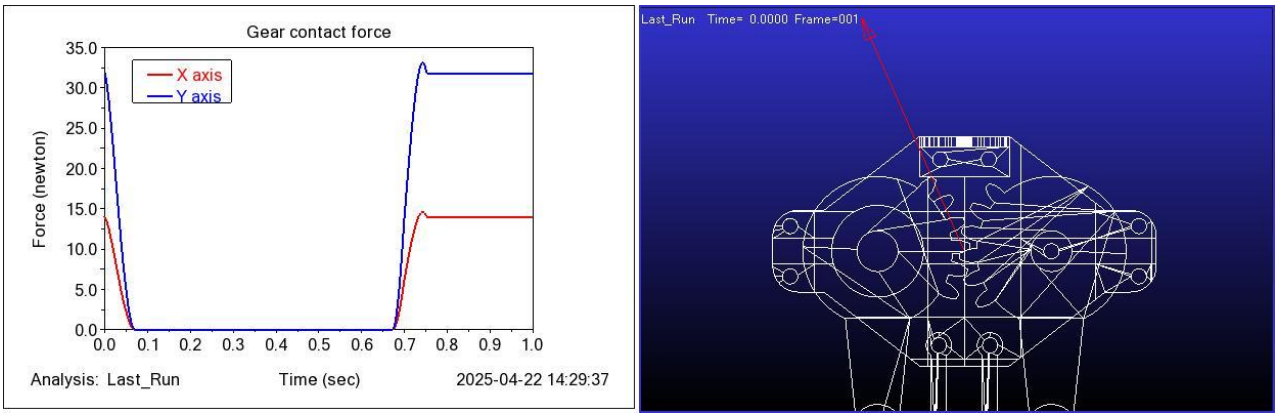

Fig. 13 -The contact force between the left and right gears

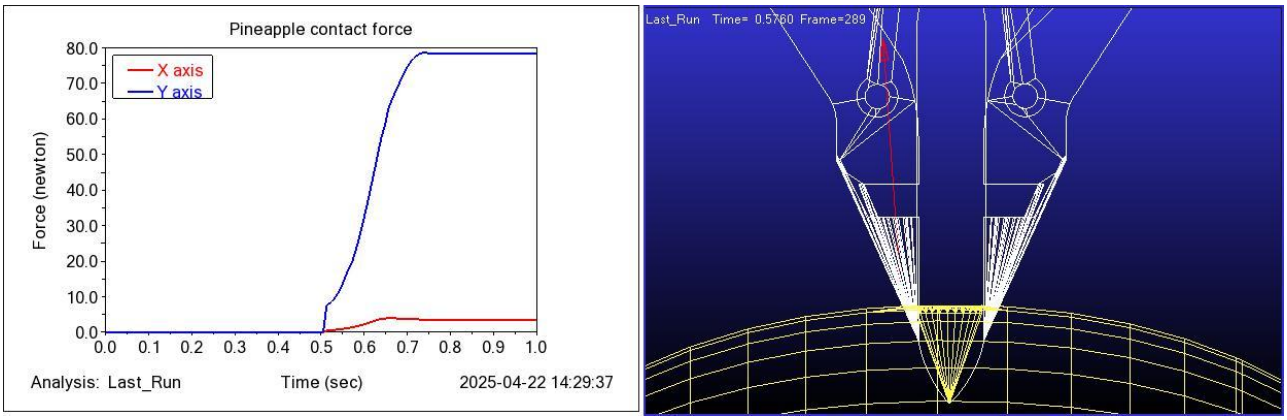

Fig. 14 -The contact force between the gripper and the pineapple flesh.

Figures 13 and 14 showed that at the instant the gripper contacted the pineapple, a contact reaction force was generated between the left and right gears, resulting in rapid contact force variation. This force changed by 33.25 N within 0.1 s. The maximum contact force between the gripper and the pineapple reached 78.64 N, with uniform overall variation, meeting the required shear force for pineapple eye removal.

To obtain the displacement curve along the eye removal direction (y-axis) and the rising phase velocity curve of the eye-removal gripper, the center of mass of the base plate and the contact point between the gripper and pineapple were analyzed. The results were shown in Figures 15 and 16.

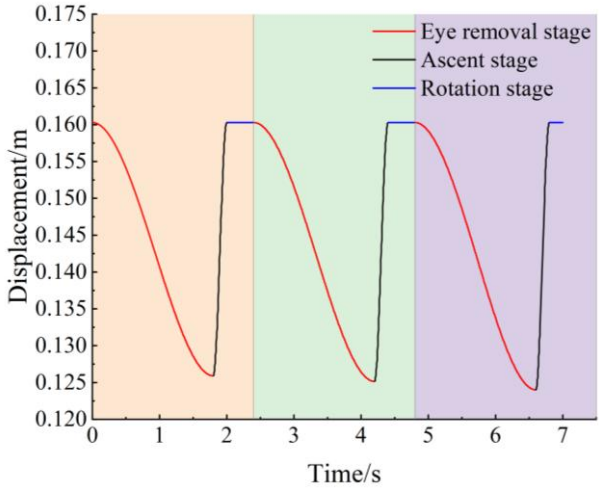

Fig. 15 -The y-axis displacement curve of the end-effector of eye removal

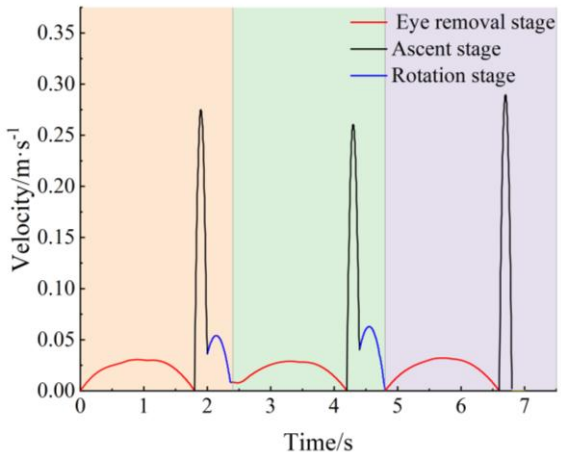

Fig. 16 - Amplification velocity curve of the pineapple-eye-removing end-effector

Figure 15 showed that during 0.0~2.4 s, the first pineapple eye (located at the center-top position) was removed, requiring the smallest downward displacement of the end-effector. From 2.4~4.8 s, the second eye (positioned laterally at a lower height) was removed, necessitating deeper end-effector displacement. During 4.8~7.0 s, the third eye (at the outermost and lowest position) was removed, demanding the maximum downward displacement. Figure 16 revealed similar velocity curves during three intervals: 0.00~1.75 s, 2.40~4.15 s, and 4.80~6.55 s, corresponding to gripper opening/closing motions for eye removal. Between 2.00~2.40 s and 4.40~4.80 s, variations occurred in the rising phase velocity of the gripper while the mechanical arm drove its rotation.

Simulation analysis of the eye removal process validated that the end-effector mechanism possessed effective displacement and velocity control capabilities during the removal of eyes at different positions. The simulation results demonstrated stable operational performance of the end-effector mechanism. The opening/closing and rotating motions of the eye-removal gripper exhibited high precision and repeatability in simulations, providing theoretical support for practical application of the device.

Finite element simulation analysis and structural optimization

To prevent stress concentration in components, ANSYS software was employed for finite element simulation analysis of the device. Aluminum alloy material properties were selected from the engineering database. Parts were discretized with a mesh size of 0.5 mm. Fixed constraints were applied to gears and the limit rocker arm, while constraint loads simulating actual working conditions were imposed. After applying all loads, the solution was computed. Total deformation contour plots and equivalent stress contour plots for the gear mechanism, limit components, and eye-removal gripper were obtained, as were shown in Figures 17-19.

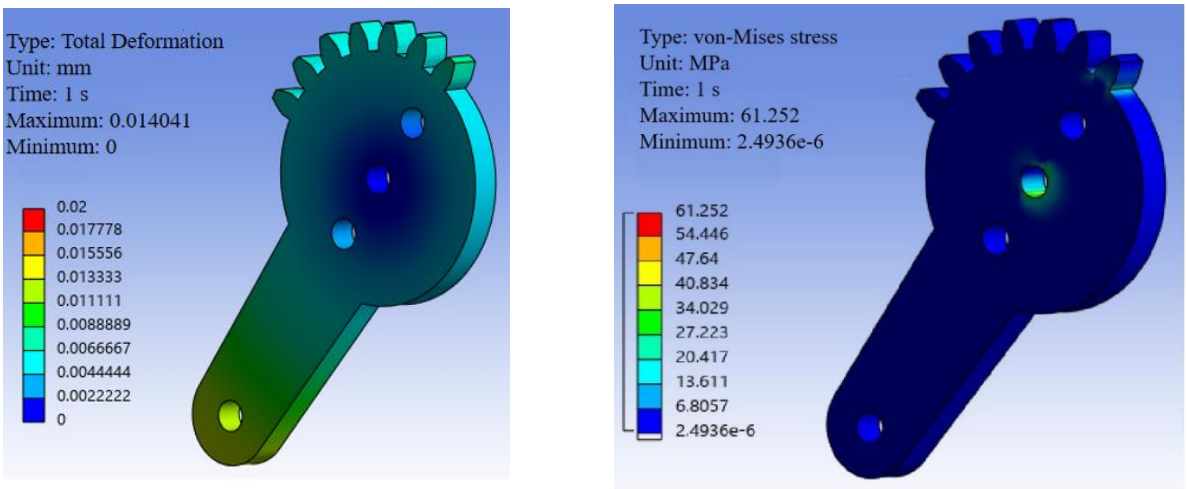

(a) (b)

Fig. 17 - Gear Mechanism Simulation Results
(a) Total deformation diagram; (b) Equivalent stress diagram

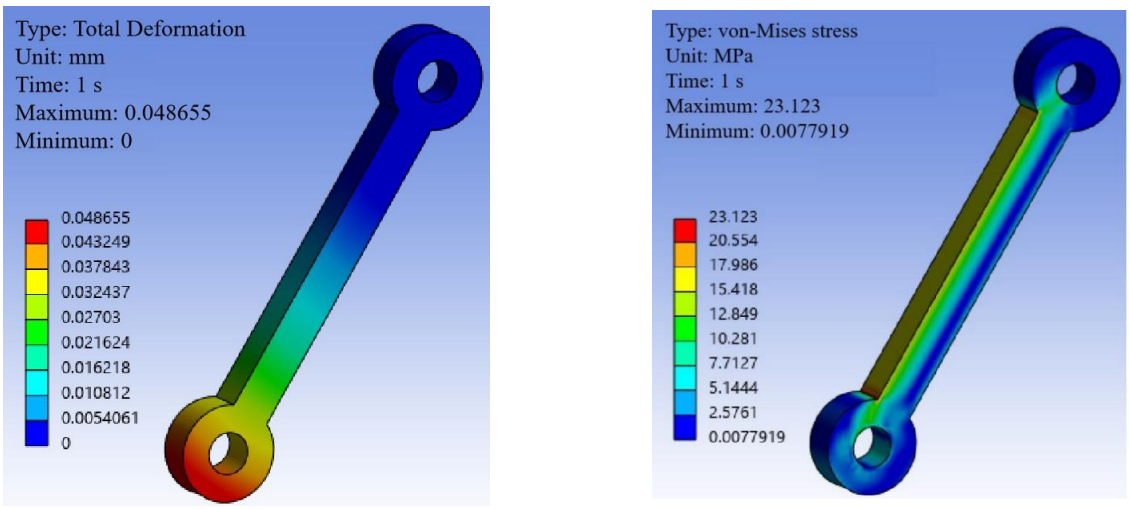

(a) **(b)**

Fig. 18 - Limiting component simulation results
(a) **Total deformation diagram**; **(b) Equivalent stress diagram**
(b)

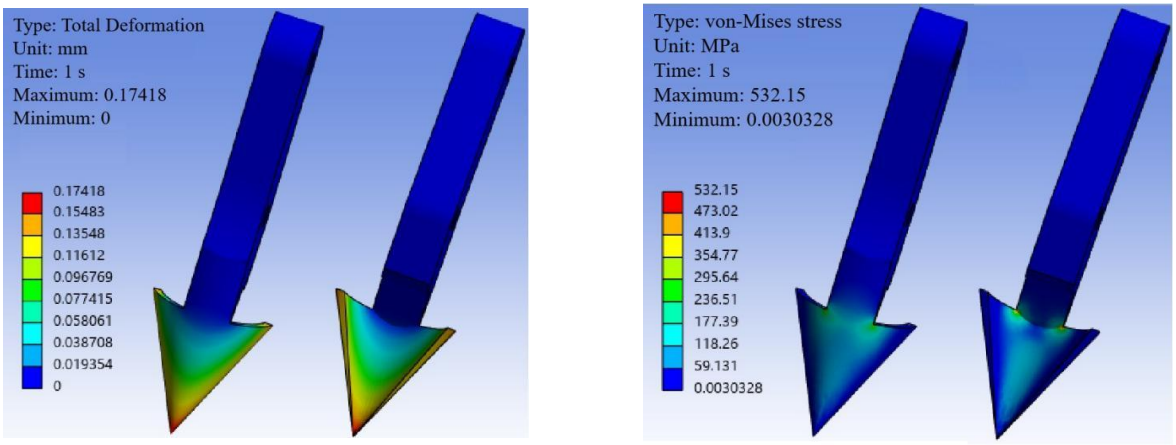

(a) **(b)**

Fig. 19 - Eye-removal gripper simulation results
(a) Total deformation diagram; (b) Equivalent stress diagram

Figures 17-19 showed that the maximum achievable stress at the gear tooth roots was 61.25 MPa, and the maximum achievable stress in the limit components was 23.12 MPa. For the eye-removal gripper, the maximum stress occurred at the blade tip, which was the contact force point with pineapple flesh, aligning with design expectations. However, the maximum deformation measured 0.17 mm and the maximum stress reached 532.15 MPa, exceeding the yield strength of aluminum alloy.

To address this issue, structural optimization was performed on the gripper. Focusing on contact force distribution, the original point-convergence blade tip design was modified to a linear-convergence configuration. By expanding the contact area with the flesh, the originally concentrated point load was distributed across a linear zone, effectively dispersing stress, improving overall load uniformity, and reducing local stress peaks. Analysis of the gripper body structure revealed insufficient wall thickness and inadequate bending stiffness. Additionally, stiffeners were confined to the transition area between the gripper and shank, leaving the main blade structure unsupported, further compromising overall rigidity. Consequently, structural improvements included thickening the main gripper body and adding cylindrical stiffeners along the curved outer edge toward the blade tip to enhance global stiffness and bending resistance. Fillet processing was applied to critical transition regions (gripper-shank junctions, stiffener-body connections) to prevent new stress concentrations at sharp corners.

The overall contour curvature and surface smoothness were optimized to improve mechanical performance and machining stability. Under identical constraints, the modified gripper was analyzed, with total deformation and equivalent stress contour plots shown in Figure 20.

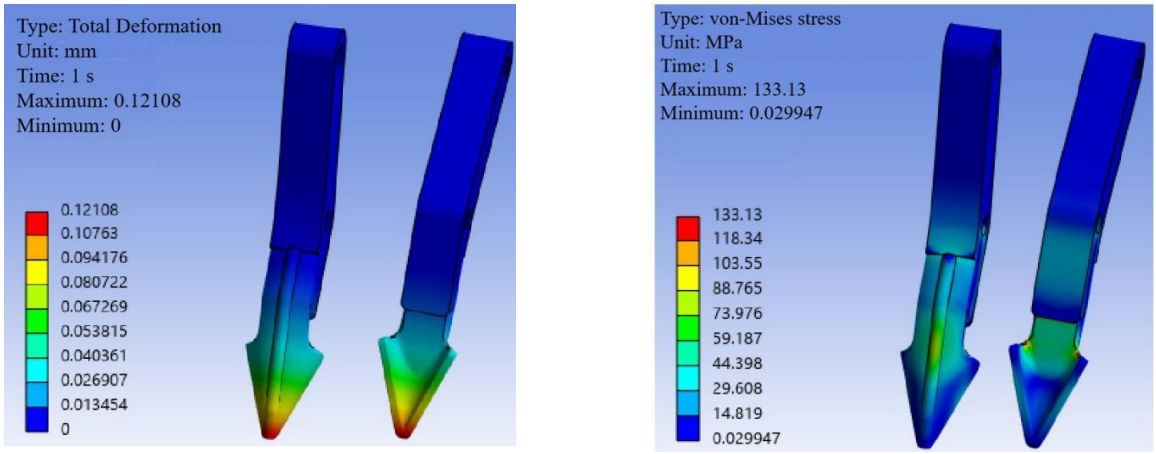

(a) **(b)**

Fig. 20 - The improved eye-removal gripper simulation results.
(a) Total deformation diagram; (b) Equivalent stress diagram

Figure 20 showed that for the optimized eye-removal gripper, deformation at the blade tip decreased from 0.17 mm to 0.12 mm, and maximum stress reduced from 532.15 MPa to 133.13 MPa, representing reductions of approximately 75% and 29.4% respectively. The maximum stress was less than the yield strength of aluminum alloy (276 MPa), satisfying structural strength and stiffness design requirements.

RESULTS AND DISCUSSION

To verify the feasibility of the end-effector mechanism, a JETSON NANO mechanical arm was selected as the execution carrier. The self-designed eye-removal end-effector mechanism was mounted at its end to construct a pineapple eye removal mechanical test device. Experimental validation was conducted as shown in Figure 21. The mechanical arm was equipped with an HTS-35H steering engine to ensure the eye-removal gripper could penetrate the eye accurately. Based on the gear torque requirement (≥105 N·mm) determined from optimal link length simulations, a TBSN-K20 steering engine was selected to provide drive power for the eye-removal gripper.

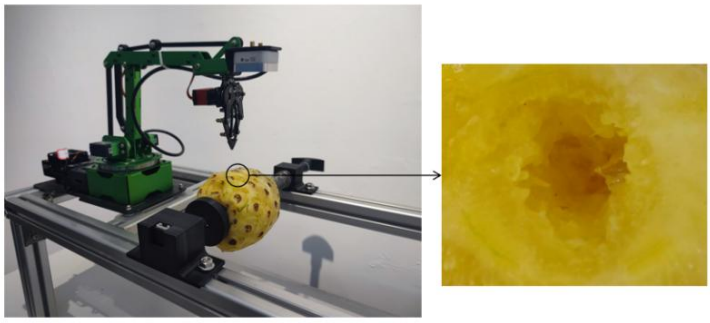

Fig. 21 - Pineapple eye removal test device and resulting eye removal effect

The experiment utilized five medium-sized pineapples at mid ripening as test materials, completing 50 eye removals total. After configuring the test device's operating program, the eye-removal gripper was manually aligned with target eyes. The automatic removal program was then executed: the mechanical arm descended autonomously with the gripper opening during descent. Upon reaching the top of the pineapple eye pit, the gripper began closing. After full closure, the mechanical arm ascended, thereby removing the eye. Experimental results were presented in Table 3.

Table 3

Eye removal test

Fruit maturation	Number of fruit eyes	The average time of eye removal[s]	Rate of success [%]
Mid ripening stage	50	2.5	98

Table 3 showed that during 50 eye removal operations by the mechanical arm with the end-effector, a success rate of 98% was achieved with an average removal time of 2.5 s per eye, validating the rationality of the structural design and operational reliability of the device. The experimental results demonstrated fundamental agreement with simulated trajectories and velocity responses, demonstrating the practical guidance value of kinematic and dynamic simulation parameters obtained from ADAMS.

ADAMS simulation results indicated an optimal driving link length of 23 mm for the end-effector mechanism. The eye removal trajectory of the gripper tip was highly consistent with the morphological contours of pineapple eyes. The maximum contact force between left/right gears reached 33.13 N, and the maximum contact force at the gripper-pineapple interface measured 78.64 N, both satisfying fundamental mechanical requirements for eye removal. However, ANSYS finite element analysis further clarified stress distribution and deformation characteristics in critical structures: the original gripper design exhibited stress concentration at the blade tip, with maximum stress reaching 532.15 MPa, exceeding the yield strength of aluminum alloy. After implementing structural optimization via blade tip modification (point-to-linear convergence), stiffener addition, and fillet processing, the maximum stress was reduced to 133.13 MPa and the deformation to 0.12 mm, thereby satisfying structural strength and stiffness requirements. Meanwhile, despite successful eye removal, the cut fruit flesh surface displayed irregularity with bruising and rough cutting surfaces. This might stem from suboptimal blade sharpness, edge angle, or material stiffness, causing excessive compression of the flesh. Additionally, the current semi-automatic test device requiring manual eye alignment exhibited low automation levels, limiting its applicability in industrial production lines.

Therefore, subsequent research would focus on two aspects: optimizing gripper material and blade edge angle to reduce flesh compression and improve cut surface smoothness, and integrating a vision module to achieve automatic eye recognition and positioning, thereby enhancing system intelligence and automation levels to provide more comprehensive technical support for practical applications.

CONCLUSIONS

Geometric characterization confirmed pineapple eyes exhibit a composite concave structure with frustum-shaped tops and conical bases. Compression tests revealed significant elastic modulus variations across pineapple regions at different ripeness levels: the core of early ripening pineapples showed the highest modulus (2.53 MPa), while late ripening flesh exhibited the lowest (0.17 MPa). The elastic modulus of eye regions in industrially preferred mid ripening pineapples (0.37 MPa) was adopted for simulations. Morphology-informed design yielded a mechanical-arm-based end-effector, with theoretical analysis establishing the gear system's minimum link length and the correlation between gear rotation and gripper opening distance. ADAMS simulations determined 23 mm as the optimal driving link length, demonstrated high consistency between the gripper tip's eye-removal trajectory and pineapple eyes' morphological contours, and confirmed maximum contact forces of 33.13 N (inter-gear) and 78.64 N (gripper-pineapple), satisfying shear removal force requirements. After structural optimization via blade tip modification (point-to-linear convergence), stiffener addition, and fillet processing, the eye-removal gripper achieved a maximum stress of 133.13 MPa and a deformation of 0.12 mm, satisfying structural strength and stiffness requirements. Experimental validation proved the design can effectively realize the pineapple eye removal operation and basically meet the design requirements. However, there is a problem of insufficient smoothness in the pit section of the eye. The follow-up research will focus on the optimization of the material and edge angle parameters of the eye-removal gripper to further improve the surface quality of the eye-removal.

ACKNOWLEDGEMENT

Thanks to the Innovation team of intelligence and key technology research for agricultural machinery and equipment in Western of Guangdong province (Grant No. 2020KCXTD039), the Key Field Project of Guangdong Provincial Universities (2024ZDZX4025), the Competitive Allocation Project of the Special Fund for Science and Technology Development of Zhanjiang City (2022A01058).

REFERENCES

[1] Deng C., Liu Y., Liang W., Ye L. (2018). Development status and countermeasures of Pineapple Industry in China (我国菠萝产业发展现状及对策). *Journal of Shanxi Agricultural Sciences*, vol. 46, no.6, pp. 1031-1034.

[2] Duan J., Wang Z., Ye L., Yang Z. (2021). Research progress and development trend of motion planning for fruit picking robotic arms (水果采摘机械臂运动规划研究进展与发展趋势). *Journal of Intelligent Agricultural Mechanization*, vol. 2, no.2, pp. 7-17.

[3] Fang W. (2023). Present situation and development suggestions of pineapple industry in Guangdong Province (广东省菠萝产业现状及发展建议). *Chinese Fruit,* no. 6, pp. 123-126.

[4] Gong M., Wang S., Ma X., Li H., Tu C., Guo Z. (2025). Design and Experiment of Pineapple Eye Removal Device Based on Machine Vision. Machines. vol. 13, no. 6, pp. 479-492.

[5] Gong Y. (2020). *Research on Strategies for Optimization and Upgrading of Pineapple Industry in Zhanjiang* (湛江市菠萝产业优化升级对策研究). MSc Thesis, Guangdong Ocean University, school of economics.

[6] Jin Y. (2021). Investigation and Analysis Report of Pineapple Market and Industry in China (我国菠萝市场与产业调查分析报告). *Market for Farm Products*, no. 8, pp. 46-47.

[7] Liu X. (2020). A Novel Pineapple Eye Removal Device (一种新型菠萝去眼器). CN211130616U, 21 Jul, 2020.

[8] Liu A., Xiang Y., Li Y., Hu Z., Dai X., Lei X., Tang Z. (2022). 3D Positioning Method for Pineapple Eyes Based on Multiangle Image Stereo-Matching. *Agriculture*, vol. 12, no. 12, pp. 2039.

[9] Liu A., Xie F., Xiang Y., Li Y., Lei X. (2024). Automatic pineapple eye removal Method and experiment based on machine vision (基于机器视觉的菠萝自动去眼方法与试验). *Journal of Agricultural Engineering*, vol. 40, no. 1, pp. 89-89.

[10] Li D., Hong K., Liu N., Wang G. (2024). Research on multi-action cooperative grasping strategy of manipulator in complex scene (复杂场景下机械臂多动作协同抓取策略方法研究). *Information and Co*ntrol, no. 4, pp. 619-631+643.

[11] Trieu N. M., Thinh N T. Pineapple Eyes Removal System in Peeling Processing Based on Image Processing[M]//Mobile Computing and Sustainable Informatics: Proceedings of ICMCSI 2022. Singapore: Springer Nature Singapore, 2022: 843-853.

[12] Kumar P. (2021). Design of Pineapple Eye-Removing Device, Advances in Manufacturing Technology and Management: *Proceedings of 6th International Conference on Advanced Production and Industrial Engineering (ICAPIE)—2021*. Singapore: Springer Nature Singapore, 2022: 142-148.

[13] Qian S., Zhao M., Chen H., Liang X., Wei Y. (2024). Method and experiment of spiral pineapple thorn removal based on 3D reconstruction (基于三维重建的菠萝螺旋去刺方法与实验). *Experimental Technology and Management*, vol. 41, no. 8, pp. 73-83.

[14] Wen B., Li C-Y. (2021). *A pineapple peel off eye integrated machine* (一种菠萝去皮去眼一体机). CN212307524U, 8 Jan, 2021.

[15] Wu Q., Wang Z., Yang Y., Lu Y., Liu G., Shi X., Bao P. (2024). Review of the development and application of mechanical arm structure (机械臂结构的发展与应用综述). *Aviation Science,* vol. 35, no.5, pp. 60-73.

[16] Xue Z., Zhang X., Chen R. (2024). Experimental study on morphology and mechanical properties of pineapple fruit (菠萝果形态及力学特性试验研究). *Journal of Agricultural Mechanization Research*, vol.46, no. 5, pp. 170-174.

[17] Xia W., Zhang Y. (2021). Research on co-simulation of six-degree-of-freedom manipulator based on SolidWorks and ADMAS (基于 SolidWorks 和 ADMAS 的六自由度机械臂联合仿真研究). *Mechanical Engineering and Automation*, no. 5, pp. 79-81.

[18] Ye M., Zhou X., Cai P., Zou H. (2011). Design of universal clamping mechanism for fruit picking robot (水果采摘机器人通用夹持机构设计). *Transactions of the Chinese Society of Agricultural Machinery*, vol.42, no.S1, pp. 177-180.

[19] Zhang D., Wang Z. (2018). Removable pineapple peel off eye integrated machine (可拆卸菠萝削皮去眼一体机). *Hebei Agricultural Machinery*, no.1, pp. 59.

[20] Zhang H., Wang Y., Hu J. (2021). Automatic pineapple eye removal device and method (菠萝自动去眼装置及菠萝自动去眼方法). CN113412954A, 21 Sep, 2021.

[21] Zhang M. (2024). Research on dual-arm collaborative control system (基于双机械臂协同控制系统的研究). *Electronic Production*, vol. 32, no. 20, pp. 29-31.